6-5-95

MICROMACHINED STIMULATING ELECTRODES

Quarterly Report #10

(Contract NIH-NINDS-N01-NS-2-2379)

January 1995 --- March 1995

Submitted to the

Neural Prosthesis Program
National Institute of Neurological Disorders and Stroke
National Institutes of Health

by the

Solid-State Electronics Laboratory
Bioelectrical Sciences Laboratory
Department of Electrical Engineering and Computer Science
University of Michigan
Ann Arbor, Michigan
48109-2122

May 1995

MICROMACHINED STIMULATING ELECTRODES

Summary

During the past quarter, research under this program has focused in a number of areas. We have modified the probe fabrication process to insert a number of inspection steps that are carried out by both the process engineer and by the designer. In addition, we have added a set of test structures to provide quantitative feedback on the process for increased process documentation and quality control. Probes produced using the new procedures have shown none of the adhesion and interfacial barrier problems experienced in the past, and we believe these problems have been eliminated using these new procedures. New instrumentation was also implemented in connection with our in-vivo current/impedance studies that provides the ability to use monopolar stimulation. It also implements *in-vivo* cyclic voltammetry (CV). Both of these new functions will allow more complete testing of the electrode sites *in vivo*. An *in vitro* test and an *in vivo* test were run to validate the new circuitry. In order to test this new instrumentation, a chronic stimulating electrode was implanted in the occipital lobe of an adult guinea pig. The electrode used was an eight-site four-shank device with site sizes of 400, 800, 1200, and 1600μm^2. Site pairs of the same size were grouped on a shank. After a 10 day rest period, the stimulation protocol began. The 1200μm^2 sites formed one bipolar pair and the 1600μm^2 sites formed a second pair. Each bipolar pair was stimulated for 3-4 hours a day for five days. The stimulus waveform was a biphasic pulse presented at 250Hz. The results of these measurements have verified the performance and capabilities of the new circuitry and will be used for detailed *in-vivo* characterization during the next quarter.

A graphical user interface is being written for use with the active stimulating probes. The graphical interface has been built around a programmable function generator paradigm. Users can specify a complete waveform by configuring individual components of the waveform (such as pulses, biphasic pulses, periods of no activity, etc.) and then sequencing them in the desired order. A sub-window will show the overall waveform as it is modified. Separate waveform specifications will occupy separate windows so that users may quickly switch between two or more waveforms. Waveform specifications may also be saved to and loaded from disk so that complicated waveforms need not be constructed anew in each session. Features such as auto-repeat and waveform chaining (starting another waveform after the current one has completed) will simplify the generation of many common waveforms.

We extensively tested all three versions of our active stimulating probes in-vitro during the past term. Both the monopolar and bipolar stimulating probes appear fully functional. Initial experiments in-vivo (in a guinea pig) have been carried out with both probes, although the initial efforts with the monopolsr probe (STIM-1b) were not successful due to non-probe-related equipment problems. STIM-1a, the bipolar probe, was tested in the dorsal cochlear nucleus of a guinea pig, and responses to stimulation were recorded from a head screw mounted on the cranium. The middle latency response (MLR) due to a bipolar biphasic (100μsec/phase) current was observed to increase with increasing current intensities and increasing site separation, as expected. In testing the full 64-site 8-channel active probe, STIM-2, a weak sinking capability was noted on many of the devices. This has been traced to process-induced variations in the device thresholds and transconductances and will be corrected on the next process run. A more robust bias string circuit is also being considered to reduce this process sensitivity in future probe designs.

MICROMACHINED STIMULATING ELECTRODES

1. Introduction

The goal of this research is the development of active multichannel arrays of stimulating electrodes suitable for studies of neural information processing at the cellular level and for a variety of closed-loop neural prostheses. The probes should be able to enter neural tissue with minimal disturbance to the neural networks there and deliver highly-controlled (spatially and temporally) charge waveforms to the tissue on a chronic basis. The probes consist of several thin-film conductors supported on a micromachined silicon substrate and insulated from it and from the surrounding electrolyte by silicon dioxide and silicon nitride dielectric films. The stimulating sites are activated iridium, defined photolithographically using a lift-off process. Passive probes having a variety of site sizes and shank configurations have been fabricated successfully and distributed to a number of research organizations nationally for evaluation in many different research preparations. For chronic use, the biggest problem associated with these passive probes concerns their leads, which must interface the probe to the outside world. Even using silicon-substrate ribbon cables, the number of allowable interconnects is necessarily limited, and yet a great many stimulating sites are ultimately desirable in order to achieve high spatial localization of the stimulus currents.

The integration of signal processing electronics on the rear of the probe substrate (creating an "active" probe) allows the use of serial digital input data which can be demultiplexed on the probe to provide access to a large number of stimulating sites. Our goal in this area of the program has been to develop a family of active probes capable of chronic implantation in tissue. For such probes, the digital input data must be translated on the probe into per-channel current amplitudes which are then applied to the tissue through the sites. Such probes require five external leads, virtually independent of the number of sites used. As discussed in our previous reports, we are now developing a series of three active probes containing CMOS signal processing electronics. Two of these probes are slightly redesigned versions of an earlier first-generation set of designs and are designated as STIM-1a and STIM-1b. The third probe, STIM-2, is a second-generation version of our high-end first-generation design, STIM-1. All three probes provide 8-bit resolution in setting the per-channel current amplitudes. STIM-1A and -1B offer a biphasic range using ±5V supplies from 0μA to ±254μA with a resolution of 2μA, while STIM-2 has a range from 0 to ±127μA with a resolution of 1μA. STIM-2 offers the ability to select 8 of 64 electrode sites and to drive these sites independently and in parallel, while -1a allows only 2 of 16 sites to be active at a time (bipolar operation). STIM-1b is a monopolar probe, which allows the user to guide an externally-provided current to any one of 16 sites as selected by the digital input address. The high-end STIM-2 contains provisions for numerous safety checks and for features such as remote impedance testing in addition to its normal operating modes. It also offers the option of being able to record from any one of the selected sites in addition to stimulation.

During the past quarter, research on this contract has focused in several areas. We have continued to fabricate passive probe structures using our new site formation techniques. New instrumentation has been developed that now allows monopolar as well as bipolar stimulation along with in-vivo CV testing of the electrodes. In-vivo and in-vitro measurements have verified this circuitry. A graphical user interface is being developed for use with the active probes. In-vitro characterization of active STIM-2 probes has continued, and in-vivo characterization using STIM-1a has begun. The results in each of these areas are described below.

2. *Passive Probe Fabrication*

During the past quarter, we have continued to fabricate passive probes for both internal and external users. This probe fabrication has been carried out using the modified site techniques described in the past quarterly report. This structure uses separate masks to define the site contact to the underlying polysilicon interconnect and to define the metal area, which overlaps the contact site. This scheme has a number of advantages. It allows a vigorous cleaning step to be carried out between the contact via formation and metal deposition, ensuring that the interconnect surface is free of polymeric films that would otherwise degrade adhesion. It also provides enhanced protection against silicon etch encroachment around the edges of the contact. Finally, it allows the site to be much wider than the interconnect, making it possible to route interconnect lines for different sites underneath the stimulating sites further up the shank. This largely uncouples the shank width from the site area and is very important given the back voltages generated when currents are driven from small sites. It has been shown that currents of 100μA will result in back voltages approaching 15V from 400μm^2 site areas, and such voltages are not attractive from the standpoints of either circuit fabrication or dielectric stress in vivo. We continue to prefer 1000μm^2 sites as representing a more appropriate design target for most neural prostheses.

During the past term, we have added several inspection points to the passive probe process and have added test structures to the mask sets to provide detailed quantitative feedback on process performance. These additions have been described in the companion quarterly report on "Thin-Film Intracortical Recording Microelectrodes" for this quarter and will not be repeated here. In probes fabricated during the past term, we have experienced no further difficulties with either the metal (site) adhesion problems nor the electrical rectification barriers we had observed on many previous fabrication efforts and feel that the new site techniques have eliminated these problems.

3. *In-Vivo Current Flow and Impedance Studies*

New instrumentation was implemented during the past term that provides the capability to stimulate monopolarly. Another new feature was a cyclic voltammetry (CV) circuit that will allow *in vivo* CV tests to be run. Both of these new functions will allow for more complete testing of the electrode sites *in vivo*. An *in vitro* test and an *in vivo* test were run to validate the new circuitry. These tests were run mainly to exercise the circuit and the software, but some information was gained in the process of verifying the new test capabilities. The results are discussed below.

The experimental protocol is summarized in Fig. 1 and will be reviewed briefly. A chronic stimulating electrode is implanted in the occipital lobe of an adult guinea pig. The electrode used in this experiment was an eight-site four-shank device with site sizes of 400, 800, 1200, and 1600μm^2. Site pairs of the same size were grouped on a shank. After a 10 day rest period, the stimulation protocol began. The 1200μm^2 sites formed one bipolar pair and the 1600μm^2 sites formed the other pair. Each bipolar pair was stimulated for 3-4 hours a day for five days. The stimulus waveform was a biphasic pulse presented at 250Hz. No evoked response was recorded for this test. The *in vitro* test followed a protocol identical to that described above except the electrode was stimulated in saline solution and the test was run for three days.

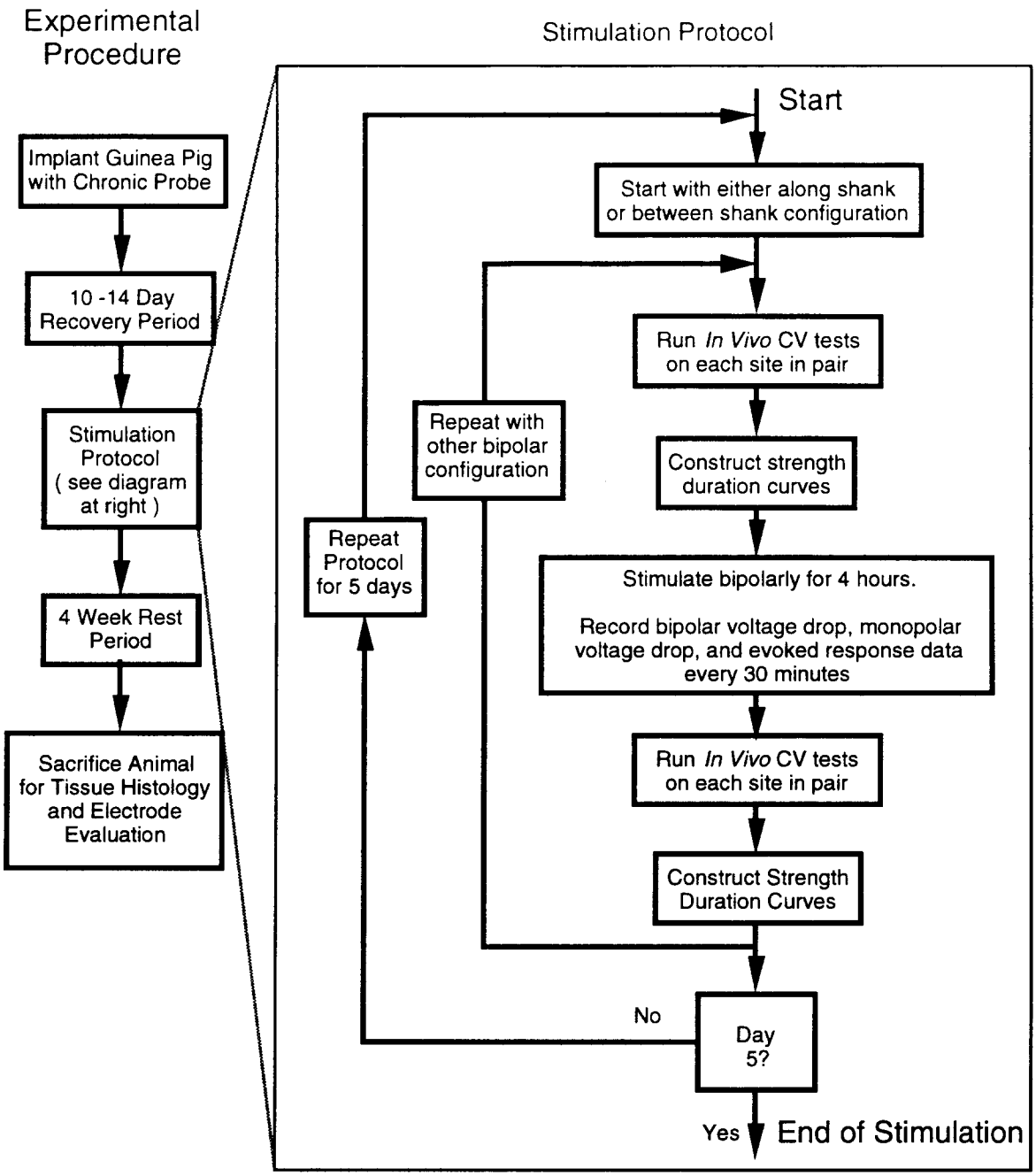

Fig. 1: Stimulation Protocol for Pulse Testing of Electrodes

The results of the CV tests during the pulse testing will be discussed first. The sites maintained a fairly constant level of charge storage capacity (CSC) during the *in vitro* test. The shape of the CV curve was also maintained. A typical CV curve is plotted in Fig. 2. The *in vivo* CV tests did not work as well. Plotted in Fig. 2 is the CV curve of site 7 of a electrode (in electrolyte) immediately after activation. The *in vivo* CV curve taken before the stimulation began is shown in Fig. 3. Unfortunately, CV tests were not run immediately after the animal was implanted, so we cannot tell if the change is due to the 10 day lag between surgery and testing, or if the *in vivo* CV method we used was

incorrect. Stainless steel head screws were used as reference and counter electrodes in a three-electrode CV configuration. We plan to consult with other investigators concerning *in vivo* CV tests. The shape of the curves seemed to change after a site was used for stimulation. Figure 4 shows that the site has a high negative current flow at the negative potential whereas before stimulation began the site had a high current flow at the positive potential. All four sites that were used to pass current exhibited this phenomenon. The two sites that were not stimulated but were tested showed no change in the shape of their CV curves. It is not certain what caused this shift.

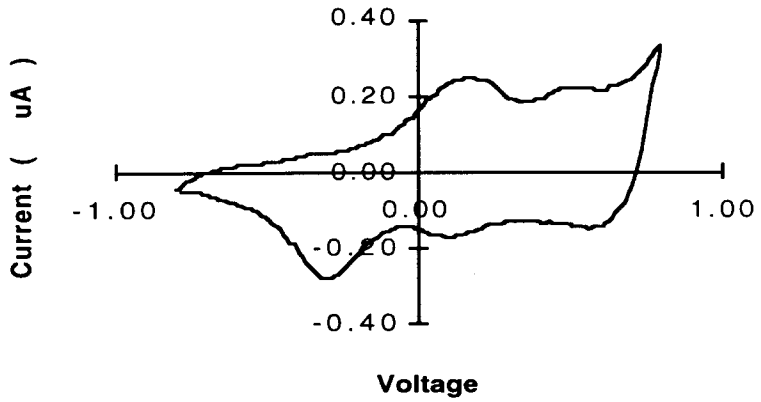

Fig. 2: *In Vitro* CV curve immediately after activation.

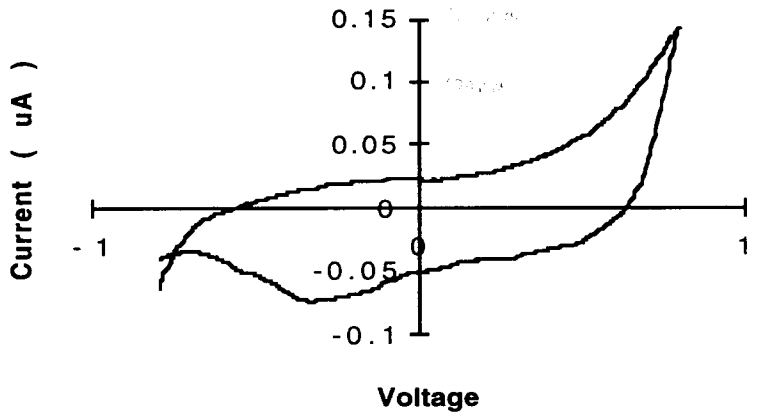

Fig. 3: *In Vivo* CV curve before any stimulation

Every 30 minutes during the stimulation period, the voltage drop across the electrode was recorded in response to a bipolar and a monopolar current pulse. It is hoped that monopolar records will provide information about the individual sites, while the bipolar data will tell about the resistance of the tissue between the two sites. Table 1 shows the monopolar access resistance and the bipolar access resistance for a day of testing. The access resistance was calculated as the initial voltage drop divided by the initial current. The difference between the sum of the two monopolar resistances and the bipolar resistance is due to the different current path forced by presence of the local current sink in the bipolar case. Both the *in vitro* and *in vivo* tests showed stable impedance and voltage drop characteristics throughout any day of testing, although the *in vivo* test showed some variation between days.

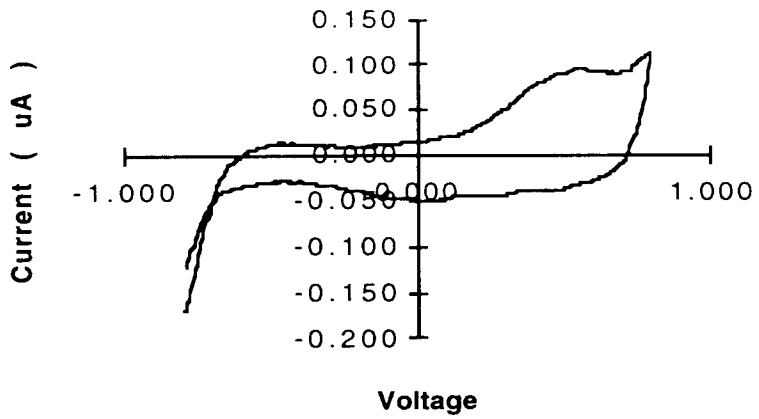

Fig. 4: *In Vivo* CV curve after 3 hours of Stimulation

Stimulation Configuration	Minutes of Stimulation						
	0	**30**	**60**	**90**	**120**	**150**	**180**
Bipolar (KOhms)	77.4	75.1	75.5	74.5	74.1	74.2	73.9
Monopole Anodic (KOhms)	28.5	27.3	28.1	27.9	27.3	28.2	28.1
Monopole Cathodic (KOhms)	37.3	35.9	36.1	36.1	35.8	35.9	35.5
Difference (KOhms)	11.6	11.9	11.3	10.5	11.0	10.1	10.3

Table 1: Access resistance for bipolar and monopolar stimulation for 3 hours of testing.

Pulse tests were run on passive stimulating electrodes *in vitro* and *in vivo*. New instrumentation was incorporated to allow us to more thoroughly test the sites during pulse tests. Some work remains in understanding *in vivo* cyclic voltammetry. During the next quarter, more animals will be implanted and stimulated tissue and implanted probes will be harvested for histology.

4. External Interface for Active Stimulating Probes

During the past few months a prototype program has been developed as an interface to an active stimulating probe. Building on the existing command-line-based interface program, the new interface is graphically oriented to allow easier interaction between human users and the probe. The programmability and flexibility of the command-line interface has not been lost, however, but simply integrated into a separate window as part of the overall interface. Thus, users can interact with the program at a graphical level (for ease of use) or at the command-line level, if greater control and programmability are desired. A typical screen shot of the program prototype is shown in Fig. 5 below.

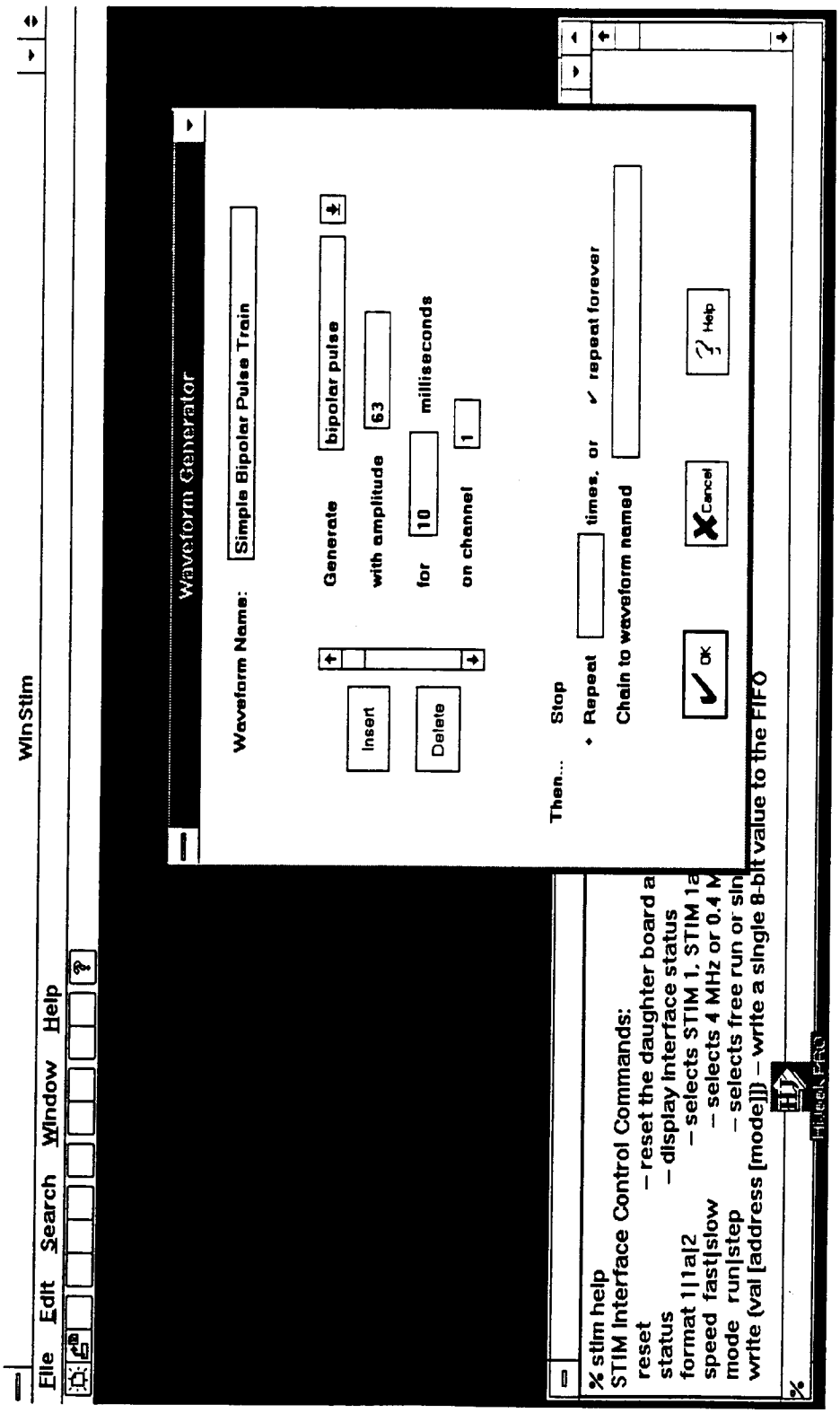

Fig. 5: Screen display for a program written as a graphical user interface for the active stimulating probes.

The graphical interface has been built around a programmable function generator paradigm. Users can specify a complete waveform by configuring individual components of the waveform (such as pulses, biphasic pulses, periods of no activity, etc.) and then sequencing them in the desired order. A sub-window will show the overall waveform as it is modified. Separate waveform specifications will occupy separate windows so that users may quickly switch between two or more waveforms. Waveform specifications may also be saved to and loaded from disk so that complicated waveforms need not be constructed anew in each session. Features such as auto-repeat and waveform chaining (starting another waveform after the current one has completed) will simplify the generation of many common waveforms.

Development of this program will go forward in parallel, however, with efforts to construct several additional external electronic interface systems for the active probes based on the prototype system which was recently completed and tested. The schematics for the circuits must be entered into a CAD system, followed by component layout and routing, and finally the printed circuit boards must be manufactured, populated with components, packaged, and tested. It is expected that these tasks will require the majority of the upcoming quarter to complete.

4. Development of Active Stimulating Probes

During the past quarter, work on the active stimulating probes focused on the in-vitro characterization of STIM-2 (the multipolar 64-site probe) and on initial work in-vivo with STIM-1a (the 16-site bipolar probe). While the monopolar and bipolar probes (STIM-1b and -1a) from the latest fabrication run have been found to work correctly with performance very close to design targets, many of the STIM-2 probes have shown a weak current sinking ability. These probes source current correctly but the sink currents are much lower than expected. We have done an extensive investigation through circuit testing and simulation to understand the origin of this problem so it can be corrected on future runs. It is not enough to fabricate a few working devices; it is essential that the circuit designs and process be robust enough to produce a high yield, consistent with delivering probes readily to internal and external users. We now understand this problem and plan to implement corrective measures in the next fabrication run.

STIM-1B

STIM-1B is the simplest version of the active stimulating probes. The probe uses a four bit counter to select one of sixteen sites. The selected site is connected to the analog data input pad through a pass-gate transistor. The counter is incremented by a positive pulse on the clock input line and can be reset to the first site by strobing the clock line negative. This monopolar probe simply performs current steering for an externally generated current. The functionality of this device is dependent primarily on correct operation of the digital logic circuitry for selecting the correct site for current delivery. The lack of any on-chip analog circuitry makes the design very robust in regard to dependence on process parameters.

The functionality of this probe after the final EDP etch and bonding was confirmed by driving the probe with a Hewlett Packard 8016A Word Generator and the interface electronics needed for generating the necessary ±5V clock signals. The probe was driven in a saline bath which was grounded by a platinum electrode in series with a 1MΩ resistor. The voltage drop across the resistor was observed on an oscilloscope. The

large resistor was used to limit current flow through the sites because the analog data line was driven with the word generator, which is essentially a voltage source.

The next obvious step in development of this probe will be *in-vivo* testing. An in-vivo test should not only show that the probe is capable of stimulating neural tissue, but that the probe is capable of producing an evoked response in up to sixteen site-specific neural tracts which we can record from further along the tract with a recording probe. Specifically, we plan to stimulate in the cochlear nucleus and, ascending the neural tract, record from the inferior colliculus or alternatively the auditory cortex. In this case, the inferior colliculus is the preferable recording site because of the higher specificity of mapping whereas the auditory cortex provides a more gross but more easily recorded response.

An attempt at performing an in-vivo experiment with this probe during the past quarter was aborted due to problems encountered during setup. One problem was related to the logistics of interfacing external electronics for both stimulation and recording with the small animal. In order to simplify this process, we anticipate adding a simple feature to the existing LabVIEW virtual instrument for recording which will allow for complete and synchronous control of stimulation and recording from the same computer. All that is required is the capability to output a ±5V pulse or pulse string to the probe clock line. We already have in place the capability to drive the probe's analog data line with a current source. This is accomplished by driving an external voltage-to-current converter with computer's D-A board. We also anticipate incorporating this simple probe controller into the activation system. As the activation process for the STIM-1b probes becomes well characterized, the controlling virtual instrument will be extended so that the sites can be automatically activated in succession without the necessity for operator intervention.

STIM-1A

STIM-1a is a first generation probe with the capability for on-chip bipolar current stimulation. The probe can source and sink current by selecting any two of its sixteen sites, one as the current source and the other as the current sink, by clocking in a fifteen bit data word and latching it with a negative clock strobe. The first four bits specify the site address of the current sink electrode, the next four bits specify the site address of the current source electrode and the last seven bits specify the amplitude of the current to be driven, which can be as high as 254μA with 2μA resolution.

The functionality of this probe was verified after the final EDP etch and the bonding step using the same method as described for STIM-1b. This probe was then tested *in-vivo* in a guinea pig. The probe was inserted into the dorsal cochlear nucleus and responses to stimulation were recorded from a head screw mounted on the cranium. We anticipated recording the middle latency response (MLR). The stimulation protocol used was a bipolar biphasic (100μsec/phase) current. Once a certain threshold level was reached, the response was observed to increase with increasing current intensities as shown in Figs. 6-9. In this case the stimulation was from sites on opposite sides of the array, therefore, with a wide separation of 1200μm. The threshold of the observable response required higher current intensity levels as site separation was decreased as can be seen by comparing Figs. 7 and 10 which show the response with 1200μm and 400μm site separation, respectively. In order to show that what was observed was actually a response and not just stimulation artifact, the animal was sacrificed without the disturbing the brain or probe and the response was again recorded. Fig. 11 shows the response just prior to sacrificing the animal and Fig. 12 shows the response just after sacrificing the

animal. The previously observed response was no longer present, indicating that the observed response was indeed of neural origin.

This experiment, though very simple, was helpful and represents the first actual use of our active stimulation probes in tissue. Actually utilizing the probe in an experimental situation has given us more insight into some of the problems in using these probes, both of a software and a hardware nature. More in-vivo experiments are planned for the coming quarter.

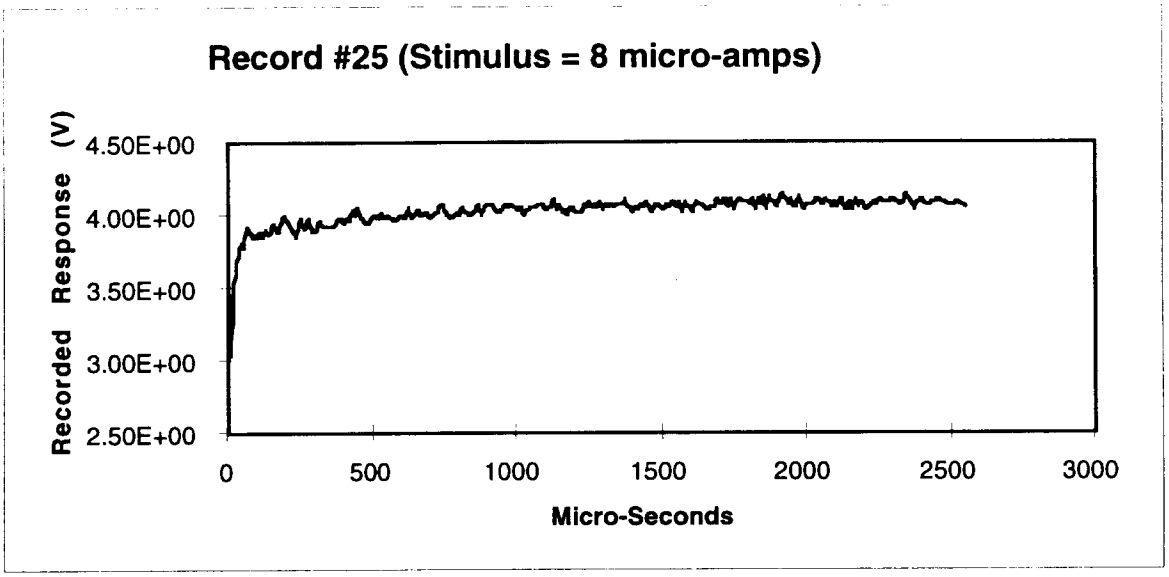

Fig. 6: The recorded response to an 8μA, bipolar, biphasic, 100μSec/phase current pulse delivered from sites on separate shanks 1200μm apart on STIM-1a.

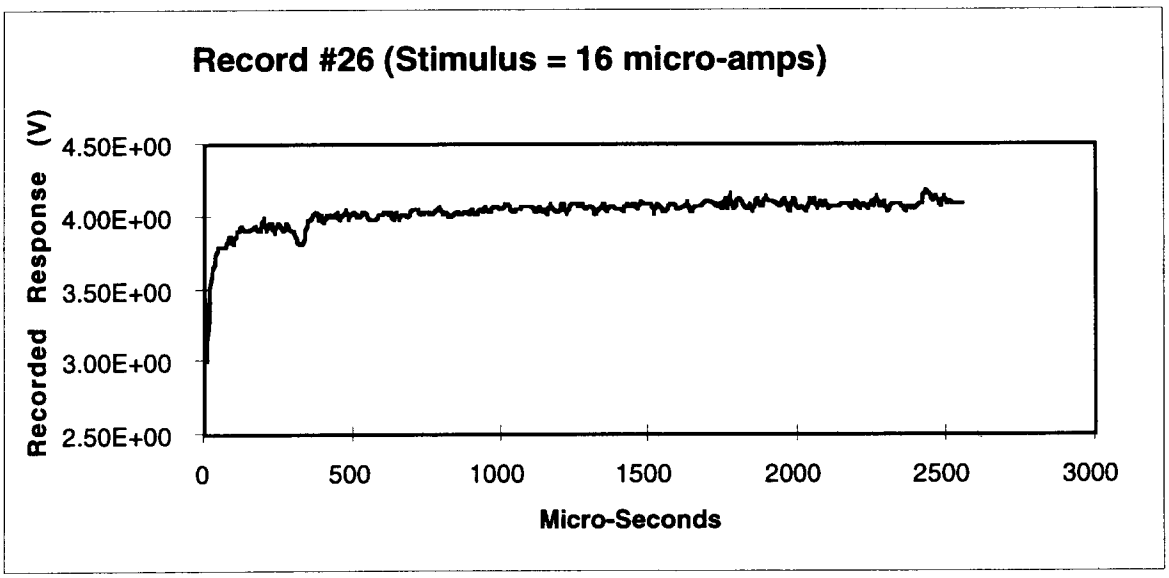

Fig. 7: The recorded response to a 16μA, bipolar, biphasic, 100μSec/phase current pulse delivered from sites on separate shanks 1200μm apart on STIM-1a.

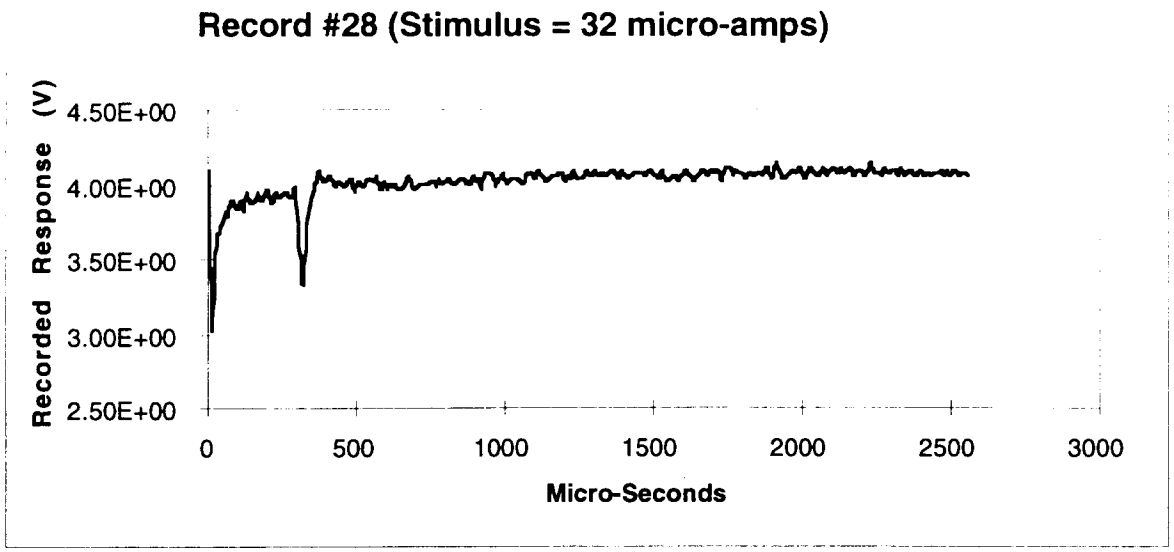

Fig. 8: The recorded response to a 32μA, bipolar, biphasic, 100μSec/phase current pulse delivered from sites on separate shanks 1200μm apart on STIM-1a.

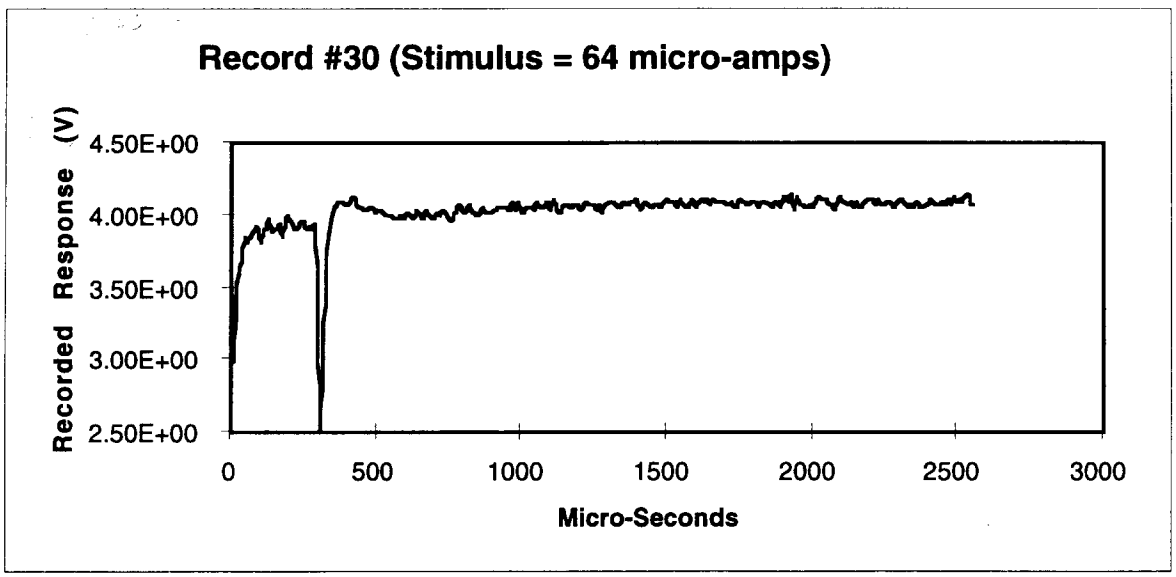

Fig. 9: The recorded response to a 64μA, bipolar, biphasic, 100μSec/phase current pulse delivered from sites on separate shanks 1200μm apart on STIM-1a.

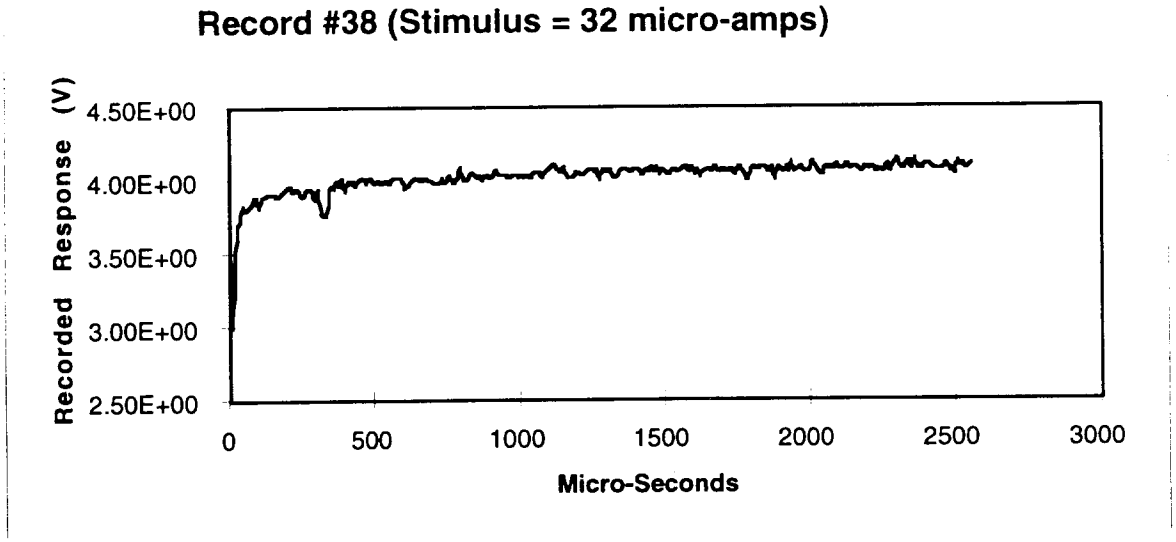

Fig. 10: The recorded response to a 32μA, bipolar, biphasic, 100μSec/phase current pulse delivered from sites on adjacent shanks 400μm apart on STIM-1a.

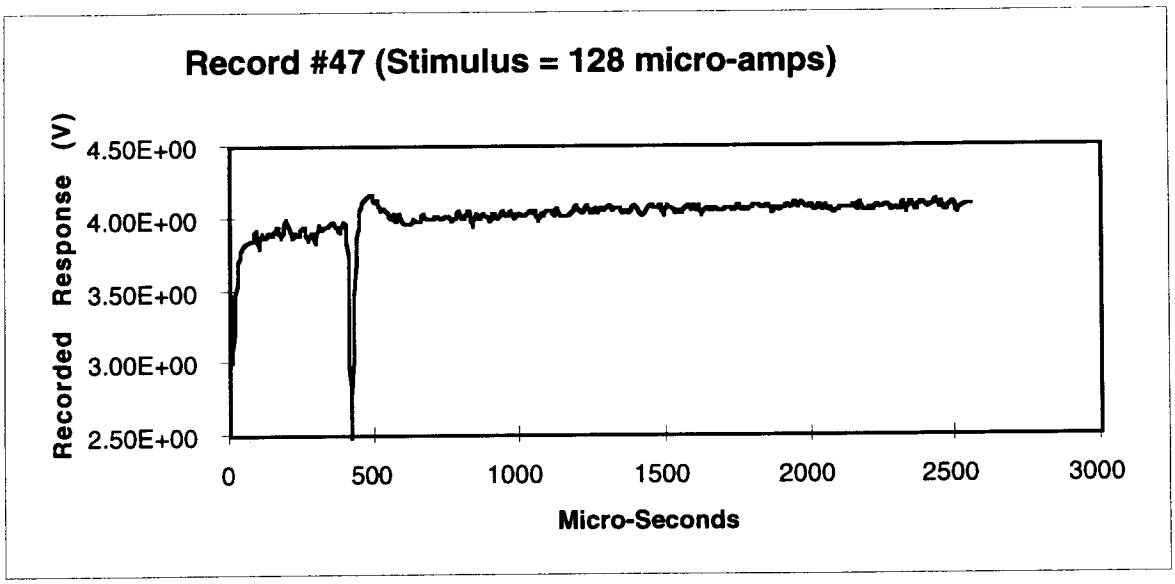

Fig. 11: The recorded response to a 128μA, bipolar, biphasic, 100μSec/phase current pulse delivered from sites on separate shanks 1200μm apart on STIM-1a just prior to sacrificing the animal.

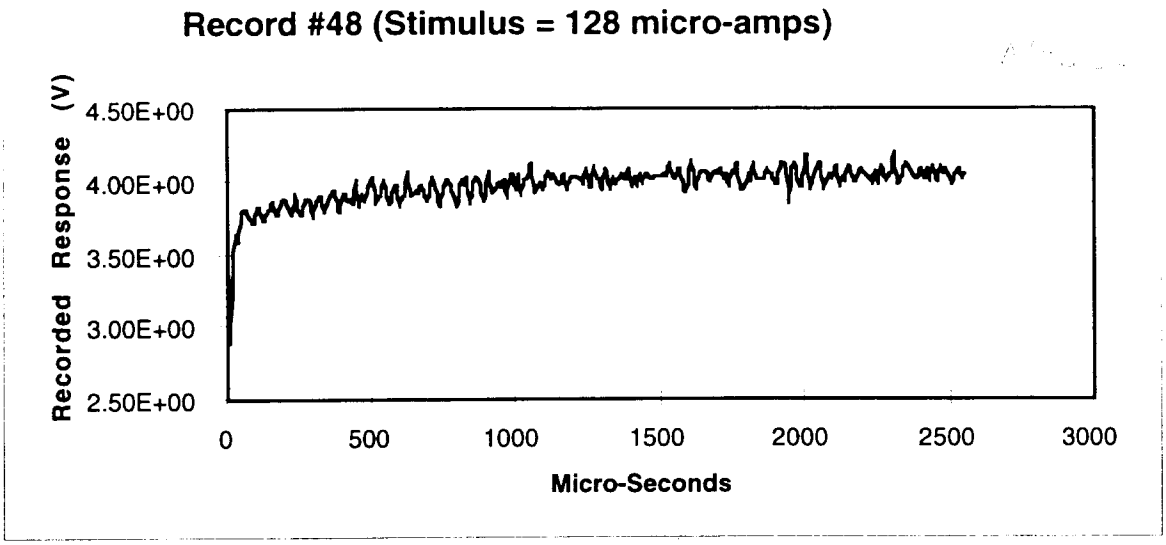

Fig. 12: The recorded response to a 128μA, bipolar, biphasic, 100μSec/phase current pulse delivered from sites on separate shanks 1200μm apart on STIM-1a just after sacrificing the animal.

STIM-2

STIM-2 is a 64-site second-generation probe that significantly extends the capabilities of the first generation probes in many areas. STIM-2 incorporates: 1) flexible interconnects to allow the rear portion of the probe to be folded flat against the cortical surface to reduce the probe height above the cortical surface; 2) new circuitry for power and area reduction with increased functionality; 3) a front-end selector which allows 8 of 64 sites to be driven simultaneously, thereby implementing electronic site positioning; and 4) compatibility with use in a multi-probe three-dimensional array.

As mentioned previously, we have noted the inability of some of the recent STIM-2 probes to sink full-scale currents. The source of this problem lies in the current sink section of the DAC current output circuitry (the NMOS device section). The first and most obvious conjecture was that this fabrication run experienced a problem such as an improper implant which resulted in NMOS devices with poor transconductance characteristics. Using an HP 4145 Parameter Analyzer, tests of the NMOS device characteristics revealed that this was not the case, as shown in Figs. 13 and 14. The threshold voltage, V_T, and the transconductance factor, K_N, were measured to be 0.698V and 54μA/V^2, respectively. K_N was determined by $K_N = g_{m,max}/V_{DS}$ where $g_m = \Delta I_{DS}/\Delta V_{GS}$ from measurement. The measured value of K_N is lower than the value that was targeted, 70μA/V^2, in the design of the NMOS devices. A look at the characteristics of the PMOS devices, shown in Figs. 15 and 16, reveals a V_T = -1V and K_P = 20.6μA/V^2 which are higher (in magnitude) and lower, respectively, than was targeted for in the design, (V_T = -0.7V and K_P = 55μA/V^2). From these characteristics, we can see that the reduced current sinking capability is not simply a result of low K_N reducing drive for the NMOS devices since the value of K_P is also reduced but the PMOS DAC still sources current quite well.

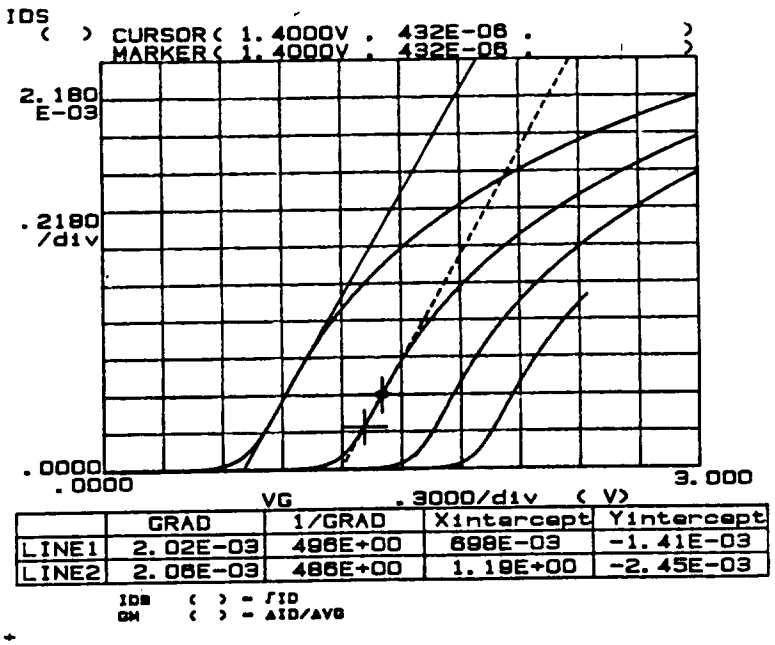

	GRAD	1/GRAD	Xintercept	Yintercept
LINE1	2.02E-03	496E+00	698E-03	-1.41E-03
LINE2	2.06E-03	486E+00	1.19E+00	-2.45E-03

IDS ( ) = ΔID
GM ( ) = ΔID/ΔVG

Fig. 13: The threshold voltage of the NMOS devices as given by the x-intercept. The different traces are from stepping the body voltage.

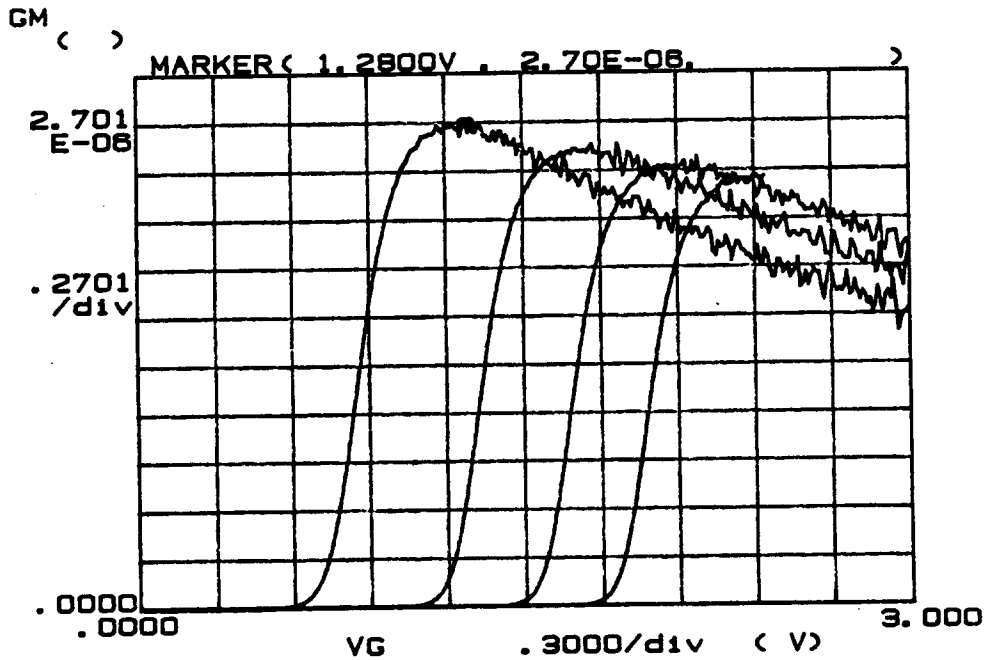

Fig. 14: The value of K_N is given by the max of g_m/V_{DS}. The effects of stepping the body voltage are also shown.

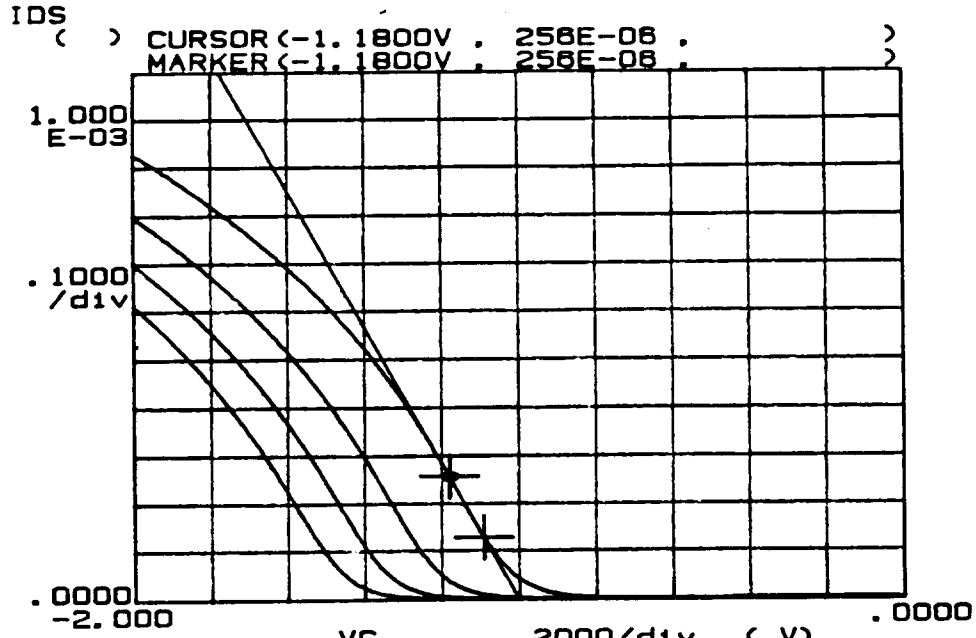

	GRAD	1/GRAD	Xintercept	Yintercept
LINE1	-1.42E-03	-706E+00	-1.00E+00	-1.42E-03
LINE2				

Fig. 15: The threshold voltage of the PMOS devices as given by the x-intercept of the tangent line. The different traces are a result of stepping the body voltage.

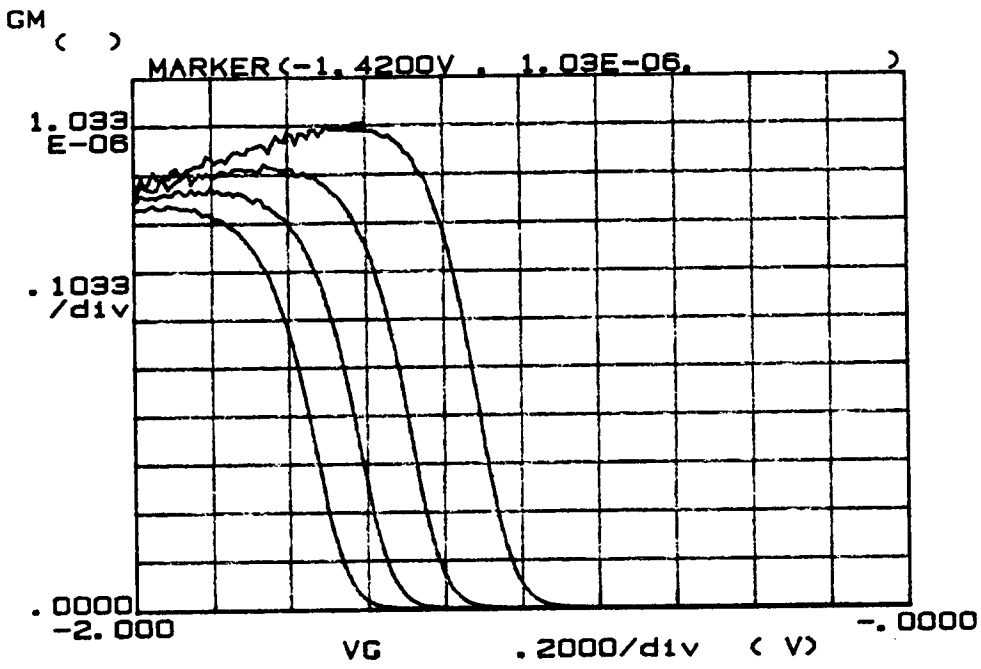

Fig. 16: The value of K_P is given by the max of g_m/V_{DS}. The effects of stepping the body voltage are also shown.

In order to observe the effect of changing the DAC bias voltage and to check the operating bias voltage, the bias node was probed and the voltage was forced over a 4V range in order to observe the characteristics of the DACs. The current delivered by the bias probe and the current delivered by the DACs were plotted versus bias voltage and are shown in Figs. 17 and 18. Note, the figures include the results of stepping the voltage at the output of the DAC. The steady state bias voltage was taken as that voltage at which the current flow in the bias voltage probe approached zero and the output current approached the value measured without a bias forcing probe. The bias points, as shown by the cursors in the graphics plots, are 2.14V and -3.87V for the current source and sink DACs, respectively. These bias points provide some of the answer to the problem. The fact that the source DAC bias point is so far from the rail explains why the PMOS devices still provide adequate current sourcing. The gate-to-source bias is very high. The opposite is true for the sinking DAC bias point; there is both a low value of K_N and a low gate-to-source voltage, both of which contribute to reducing the current. This all points to a problem with the bias transistor string or the reference current portion of the current mirror. The question is why the current is so much lower on the NMOS side of the DAC (sink) than on the PMOS side (source). The answer appears to be in the mismatched threshold voltages and reduced K values, which are a result of process variations. The reduced K values are primarily a result of a much thicker gate oxide, 430Å as opposed to the 300Å target. The increased gate oxide thickness also has an effect on the thresholds, but they are primarily a set by threshold ion implants, which were deliberately spread over a range in the wafers processed. We are currently modifying our process to tighten up controls over both the gate oxide thickness and the thresholds. We are also looking to design a more robust and less process dependent reference current leg for the DACs. The present design uses transistors in the bias string with length-to-width ratios as high as 30:1. While this results in very low string bias currents and a low overall power dissipation for the probe (the reference currents are targeted at 1μA), it also makes the bias points sensitive to process variations and to field leakage currents. Physically smaller transistors having lower (L/W) ratios and higher bias currents would help this situation and will be included in the next design iteration for this probe.

During the coming quarter, we plan to etch out more of the STIM-1b and STIM-1a probes. We expect to increase our utilization of these probes in actual experiments as we become more familiar with them and improve our external system capabilities. We also expect to finalize the solution to the STIM-2 current sinking problem and produce more robust working probes of this type. We also anticipate the development of the simple probe controller virtual instruments for all of the probe designs to be used in conjunction with the activation and recording systems.

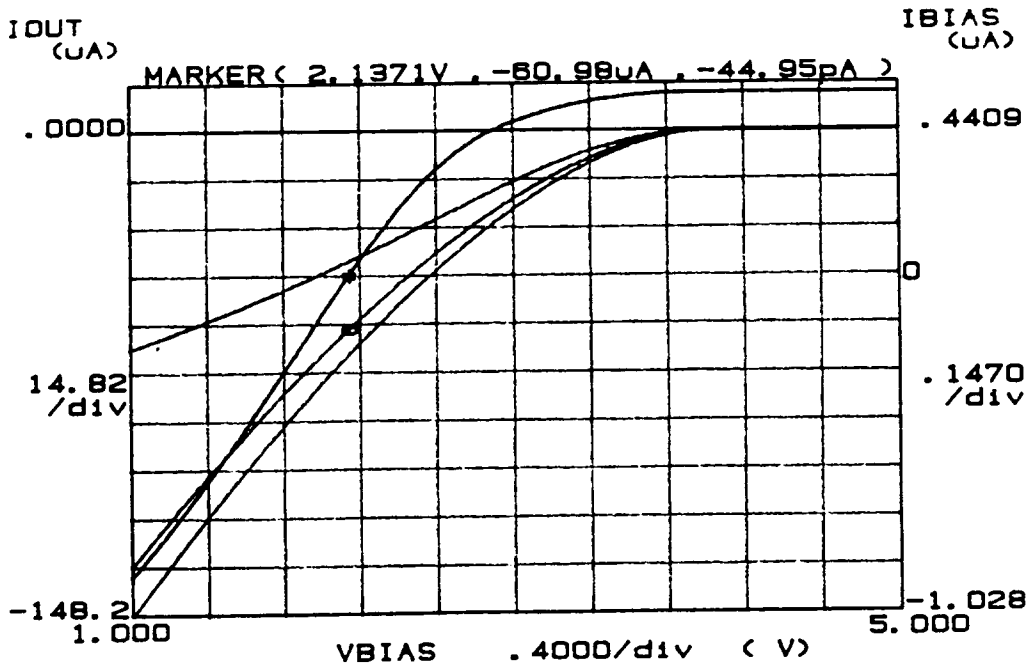

Fig. 17: The current sourcing capability of the PMOS DAC and the probing current versus bias voltage. The shows the bias point (zero probe current) and the capability of the DAC at different bias points. Steps in voltage at the DAC output are also shown.

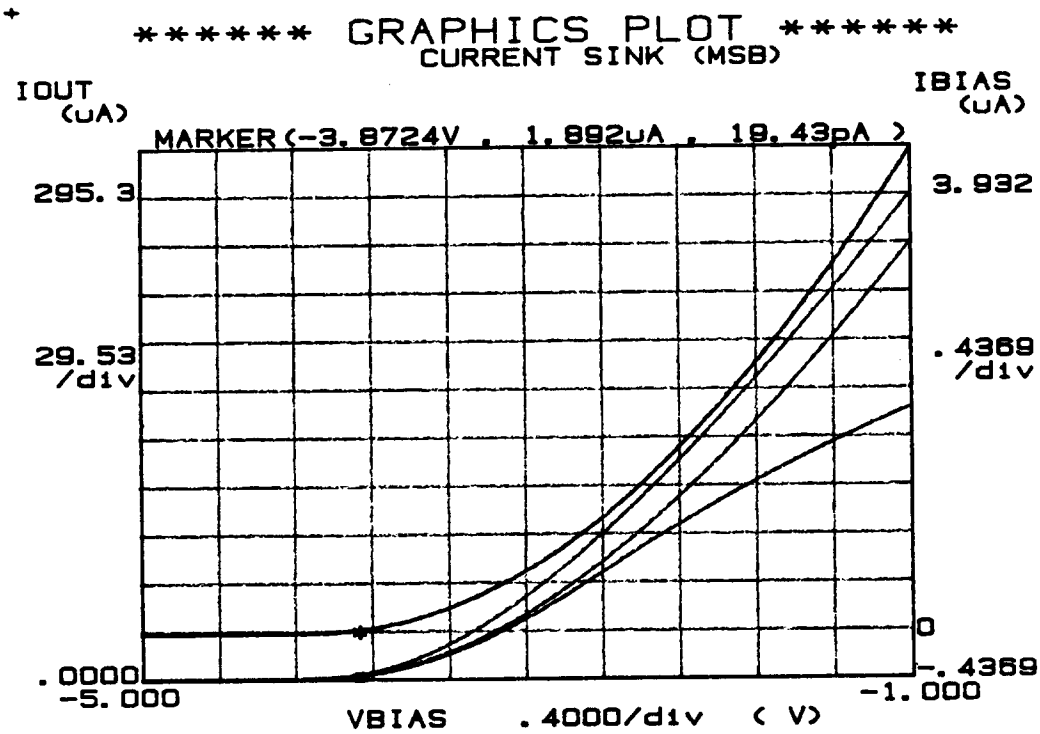

Fig. 18: The current sourcing capability of the NMOS DAC and the probing current versus bias voltage. The shows the bias point (zero probe current) and the capability of the DAC at different bias points. Steps in voltage at the DAC output are also shown.

5. *Conclusions*

During the past quarter, research under this program has focused in a number of areas. We have modified the probe fabrication process to insert a number of inspection steps that are carried out by both the process engineer and by the designer. In addition, we have added a set of test structures to provide quantitative feedback on the process for increased process documentation and quality control. Probes produced using the new procedures have shown none of the adhesion and interfacial barrier problems experienced in the past, and we believe these problems have been eliminated using these new procedures. New instrumentation was also implemented in connection with our in-vivo current/impedance studies that provides the ability to use monopolar stimulation. It also implements *in-vivo* cyclic voltammetry (CV). Both of these new functions will allow more complete testing of the electrode sites *in vivo*. An *in vitro* test and an *in vivo* test were run to validate the new circuitry. In order to test this new instrumentation, a chronic stimulating electrode was implanted in the occipital lobe of an adult guinea pig. The electrode used was an eight-site four-shank device with site sizes of 400, 800, 1200, and 1600μm^2. Site pairs of the same size were grouped on a shank. After a 10 day rest period, the stimulation protocol began. The 1200μm^2 sites formed one bipolar pair and the 1600μm^2 sites formed a second pair. Each bipolar pair was stimulated for 3-4 hours a day for five days. The stimulus waveform was a biphasic pulse presented at 250Hz. The results of these measurements have verified the performance and capabilities of the new circuitry and will be used for detailed *in-vivo* characterization during the next quarter.

A graphical user interface is being written for use with the active stimulating probes. The graphical interface has been built around a programmable function generator paradigm. Users can specify a complete waveform by configuring individual components of the waveform (such as pulses, biphasic pulses, periods of no activity, etc.) and then sequencing them in the desired order. A sub-window will show the overall waveform as it is modified. Separate waveform specifications will occupy separate windows so that users may quickly switch between two or more waveforms. Waveform specifications may also be saved to and loaded from disk so that complicated waveforms need not be constructed anew in each session. Features such as auto-repeat and waveform chaining (starting another waveform after the current one has completed) will simplify the generation of many common waveforms.

We extensively tested all three versions of our active stimulating probes in-vitro during the past term. Both the monopolar and bipolar stimulating probes appear fully functional. Initial experiments in-vivo (in a guinea pig) have been carried out with both probes, although the initial efforts with the monopolar probe (STIM-1b) were not successful due to non-probe-related equipment problems. STIM-1a, the bipolar probe, was tested in the dorsal cochlear nucleus of a guinea pig, and responses to stimulation were recorded from a head screw mounted on the cranium. The middle latency response (MLR) due to a bipolar biphasic (100μsec/phase) current was observed to increase with increasing current intensities and increasing site separation, as expected. In testing the full 64-site 8-channel active probe, STIM-2, a weak sinking capability was noted on many of the devices. This has been traced to process-induced variations in the device thresholds and transconductances and will be corrected on the next process run. A more robust bias string circuit is also being considered to reduce this process sensitivity in future probe designs.